ORNL/TM-2022/2554

Engineering-Scale Batch Purification of Ternary $MgCl_2$-KCl-NaCl Salt Using Thermal and Magnesium Contact Treatment

Kevin R. Robb
Seth Baird
Jordan Massengale
Nathaniel Hoyt
Jicheng Guo
Colin Moore

August 2022

OAK RIDGE National Laboratory

ORNL IS MANAGED BY UT-BATTELLE LLC FOR THE US DEPARTMENT OF ENERGY

ORNL/TM-2022/2554

Nuclear Energy and Fuel Cycle Division

ENGINEERING-SCALE BATCH PURIFICATION OF TERNARY $MgCl_2$-KCl-NaCl SALT USING THERMAL AND MAGNESIUM CONTACT TREATMENT

Kevin R. Robb, Seth Baird, Jordan Massengale

Oak Ridge National Laboratory

Nathaniel Hoyt, Jicheng Guo, Colin Moore

Argonne National Laboratory

August 2022

Prepared by
OAK RIDGE NATIONAL LABORATORY
Oak Ridge, TN 37831
managed by
UT-BATTELLE LLC
for the
US DEPARTMENT OF ENERGY
under contract DE-AC05-00OR22725

CONTENTS

LIST OF FIGURES

LIST OF TABLES

ABSTRACT

High-temperature molten chloride salts are a desirable heat transfer and energy storage media. The NaCl-KCl-$MgCl_2$ salt is of particular interest because of its low melting point and relatively inexpensive constituents. Moisture and hydroxides must be removed from the salt to control corrosion at high temperatures. Previous studies have developed and demonstrated various techniques for bench-scale salt purifications. This paper details the system, process, and insight gained in the purification of a 200 kg scale batch of NaCl-KCl-$MgCl_2$ salt at Oak Ridge National Laboratory.

1. BACKGROUND

Molten chloride salts are a leading candidate for heat transfer and thermal energy storage media for next-generation concentrating solar power (CSP) and molten salt nuclear reactors. For CSP applications, the NaCl-KCl-$MgCl_2$ ternary salt has many advantages, including the low cost of the raw materials and its low melting point compared with alternative salt blends. Despite its potential, molten chloride salt technology is at an early stage of technology readiness with respect to energy system deployment. The Facility to Alleviate Salt Technology Risks (FASTR) was designed and constructed to advance this technology [1]. FASTR includes a salt purification system and a high-temperature pumped flow loop. The purification system provides the 120 L of purified NaCl-KCl-$MgCl_2$ ternary salt required by the flow loop.

Anhydrous chloride salts, particularly $MgCl_2$, readily absorb moisture. Moisture and hydroxides increase corrosion rates between high-temperature molten chloride salt and salt-wetted structures. The complex hydrated salts of $MgCl_2$ (e.g., $MgCl_2$•$6H_2O$, $MgCl_2$•$4H_2O$, $MgCl_2$•$2H_2O$) are dehydrated at elevated temperatures, liberating H_2O. However, $MgCl_2$•$2H_2O$ and $MgCl_2$•H_2O, can undergo partial hydrolysis, forming MgOHCl and HCl, as shown in Eqs. (1)–(4) [2 ,3]. At elevated temperatures, MgOHCl thermally decomposes into MgO and HCl, as shown in Eq. (5). Neither of these products are desired and result in lowering the $MgCl_2$ content of the salt. HCl, in particular, is corrosive both within the liquid salt and in the vapor headspace in its gaseous form. Successful removal of MgOHCl therefore requires a process other than heating the salt.

$$MgCl_2 \cdot 2H_2O \rightarrow MgCl_2 \cdot H_2O + H_2O \qquad 153–242°C \qquad (1)$$

$$MgCl_2 \cdot H_2O \rightarrow MgCl_2 + H_2O \qquad 304–400°C \qquad (2)$$

$$MgCl_2 \cdot 2H_2O \rightarrow MgOHCl + HCl + H_2O \qquad 193–240°C \qquad (3)$$

$$MgCl_2 + H_2O \rightarrow MgOHCl + HCl \qquad 210–445°C \qquad (4)$$

$$MgOHCl \rightarrow MgO + HCl \qquad 533–568°C \qquad (5)$$

At the outset of the FASTR project, the method for chloride salt preparation was not defined. At the time, Oak Ridge National Laboratory (ORNL) was purifying chloride salts to oxide concentrations below 200 micromolal (micromoles of MgO per kilogram of salt) through carbochlorination using CCl_4 as the reagent [4, 5]. Carbochlorination has been used at the industrial scale to purify $MgCl_2$ through sparging Cl_2 gas in the presence of a separate C source. The choice of CCl_4 was motivated by the thermodynamics discussed in Kurley et al. [5], which demonstrated that sparging HCl alone is insufficient to remove MgO. Furthermore, a researcher previously demonstrated the improved efficacy of purifying KCl-$MgCl_2$ with CCl_4 compared with using HCl in Ambrosek [6]. Concurrent to the use of CCl_4, ORNL also investigated a potential lower temperature purification process using $SOCl_2$ [7]. However, the limited study identified further research required to develop the process.

An alternative process is to contact the salt with metallic Mg to reduce HCl and MgOHCl impurities [3]. As shown in Eq. (6), the reaction leads to the formation of H_2. Variations in this approach have been used historically to purify NaCl-KCl-$MgCl_2$ [8, 9, 10] and KCl-$MgCl_2$ [6]. Although this reaction results in MgO particles, these particles can be readily removed via filtration or other methods. Furthermore, adding excess Mg to the salt sets a low redox potential. The efficacy of adding Mg to chloride salt has been demonstrated in its ability to purify the salt [3], reduce and maintain the salt redox potential [11, 12], and decrease corrosion in isothermal static corrosion tests [6, 13, 14, 15], as well as in flowing systems with a temperature differential [13, 16].

$$2MgOHCl + Mg \rightarrow 2MgO + MgCl_2 + H_2 \quad (6)$$

The processes discussed all have advantages and disadvantages related to handling hazardous reagents, managing hazardous effluent, and scaling the process. Ultimately, with the input from a consortia of US national laboratories—including ORNL, Savanah River National Laboratory, National Renewable Energy Laboratory, and Argonne National Laboratory (ANL)—researchers decided to pursue the Mg contact method of purification. The consortia defined a standardized purification procedure in 2018 (Appendix A of Pint [13]). This procedure, defined for batch sizes of approximately 1 kg scale, served as the starting point for scaling up the process to the 200 kg batch size required for FASTR.

2. EXPERIMENTAL FACILITY AND MATERIALS

The salt purification system is housed within a ventilated enclosure, as shown in Figure 1. An alloy C-276 vessel serves as the pressure boundary for the purification process. The 2.5 m (88.5 in.) tall, 0.508 m (20 in.) outside diameter vessel houses a liner with a 0.464 m (18.25 in.) inner diameter. The C-276 liner prevents molten salt from contacting the pressure boundary. The processing vessel cylindrical surface is heated externally using insulated heater blankets. The heater blankets are divided into three independently controlled zones in the axial direction. The bottom of the vessel rests on a custom heater plate with embedded cartridge heaters. A trace heater element and 2 in. of higher-temperature insulation rest atop the vessel lid.

Figure 1. Purification system.

A 12.7 mm (0.5 in.) alloy C-276 sparger tube extends into the processing vessel, terminating approximately 38.1 mm (1.5 in.) from the bottom. Ultrahigh purity (UHP) Ar is fed into the sparger tube to agitate the molten salt. A separate flow of UHP Ar is fed into the head space of the processing vessel to help sweep the process effluent from the vessel. Before entering the vessel, the UHP Ar is passed through a commercial molecular sieve to further reduce the introduction of impurities.

The effluent from the process exits through a 12.7 mm (0.5 in.) alloy C-276 line that is heated to 140°C. The effluent then passes through a scrubber to capture HCl. The scrubber comprises four plastic bottles connected in series. The first bottle serves as a vacuum break and was prefilled with 1 L of demineralized water (i.e., 18 MΩ). The second, third, and fourth bottles each have a 4 L capacity and were initially filled with 2.5, 2, and 2 L of demineralized water, respectively. The effluent is bubbled through a 6.35 mm (0.25 in.) line in the last three scrubber bottles before exiting. After the scrubber, the flow passes through a flame arrestor before being released to the ventilated enclosure.

At the end of the process, a 12.7 mm (0.5 in.) alloy C-276 transfer line was inserted into the vessel to transfer salt from the processing vessel into an alloy C-276 storage vessel shown on the left in Figure 1. The transfer line included three mechanical filters in series. The filters were made of woven 316 stainless-steel mesh with nominal apertures of 40, 25, and 5 μm.

The process is controlled and monitored by a range of instrumentation. The gas injected into the bubbler tube and head space of the processing vessel is controlled by mass flow controllers and monitored with pressure transducers. Many type-N thermocouples were used to monitor system temperatures. The heater blankets and underlying heater plate house 10 thermocouples. Three thermocouples in an Alloy 600 thermowell extended into the processing vessel with two in the gas space and one at the top of the loaded salt. Additionally, trace heated lines—the off-gas line and transfer line—were instrumented with thermocouples. The off-gas line between the processing vessel and the scrubber is monitored with a residual gas analyzer (RGA model ThinkSRS UGA100) and a humidity sensor (Vaisala HMT334). The capillary tube between the off-gas line and the RGA was heated to 100°C. A pH sensor (Valmet 4338) is used to monitor the pH of the scrubber. Through appropriately aligning hand valves, samples from either the first or second scrubber are pumped through the sensor before being returned to the scrubber. A custom electrochemical sensor, developed at ANL, was used to monitor the salt potential.

The salt is a blend of two industrially sourced salts: anhydrous carnalite (AC) from Israel Chemicals Ltd. (ICL) and Silver Peak (SPK) halite from Albemarle Inc.. Both salts were visually and chemically heterogenous. ICL provided a batch analysis report for the AC salt: 20.7K–12.0Mg–4.84Na–58.7Cl–2.49H_2O (wt %). There is a low melting point eutectic of approximately 387°C for the ternary 20.5KCl–24.5NaCl–55.0$MgCl_2$ (wt %) [17]. The goal was to mix the two industrial salts to arrive at a low-melting composition. Magnesium (Sigma-Aldrich turnings, 5–25 mm, 99.95% trace metals basis) was also used during the purification process.

3. PROCESS

The process was intentionally protracted for several reasons. Although the goal was to purify the salt, there was a concerted effort to collect data to advance the understanding of the effect of processing variables on the process. Concurrent data analysis and consultations with off-site experts were compared against expectations and used to inform the next steps. Finally, this was the first operation, and several hardware and process events required attention before proceeding to the next step. Ultimately, the information obtained can be used to optimize and accelerate the process in the future.

The overall process can be divided into four segments. First, the salt was loaded into the processing vessel. The vessel was sealed and heated while under a continuous flow of Ar. The applied heating schedule, as well as the nominal sweep and sparging gas flow rates during those periods, are summarized in Table 1. The heating schedule can be divided into a low-temperature period before the salt is molten and a high-temperature period during which the salt was molten. Finally, once the salt was deemed purified, it was transferred to a storage tank. The four periods are discussed in the following sections.

Table 1. Set temperature vs. time summary for the process.

Step	Temperature ramp (°C)	Hold time (h)	Sweep gas flow rate (slpm)	Sparger gas flow rate (slpm)
1	25 → 250	75	3.0–2.0	3.0–2.0
2	250 → 300	91	2.5	1.5
3	300 → 500	67	2.5	1.5
4	500 → 555	38	2.0	2.0
5	555 → 530	41	3.75–2.0	1.25–2.0
6	530 → 555	19	2.0	2.0
7	555 → 630	3	2.0	2.0
8	630 → 610	14	2.0	2.0
9	610 → 675	10	2.0	2.0
10	675 → 555	43	2.0–1.0	2.0–0.25

3.1 SALT LOADING

The 198.7 kg of ICL AC was first loaded in the processing vessel liner, followed by 13.5 kg of the Albemarle halite. The 212.2 kg of loose-filled salt had a relatively high effective density of 1,485 kg/m^3. A total of 241 g of Mg were initially added to the salt (0.11 wt %). Two C-276 mesh bags encased 137 g and were hung using alloy 600 wire inside the vessel toward the bottom during salt loading. The remaining 104 g of Mg were added as loose pieces after approximately half of the salt was loaded. The vessel lid was then placed and sealed and the remaining tubing connections completed. The vessel was held at 25°C for over 16 h with a 1.5 slpm flow of Ar through the sweep line. This facilitated initial inerting of the processing vessel through at least 4.5 volume changes. Additional leak checks of the vessel were also conducted during this time.

3.2 LOW-TEMPERATURE PROCESS

After the 25°C hold, the vessel was brought to and held at the intermediate temperatures of 250°C and then 300°C for approximately 7 days. Figure 2 shows the time evolution of the system temperatures, humidity signal, RGA data, and the estimated HCl captured in the first scrubber. The reference time of 0 h corresponds to the start of the ramp to 250°C. The vessel temperatures were measured on the outside of the tank, whereas the temperature of the top of the salt was measured inside the vessel. During the high-temperature process, this thermocouple had to be removed to enable additions of Mg.

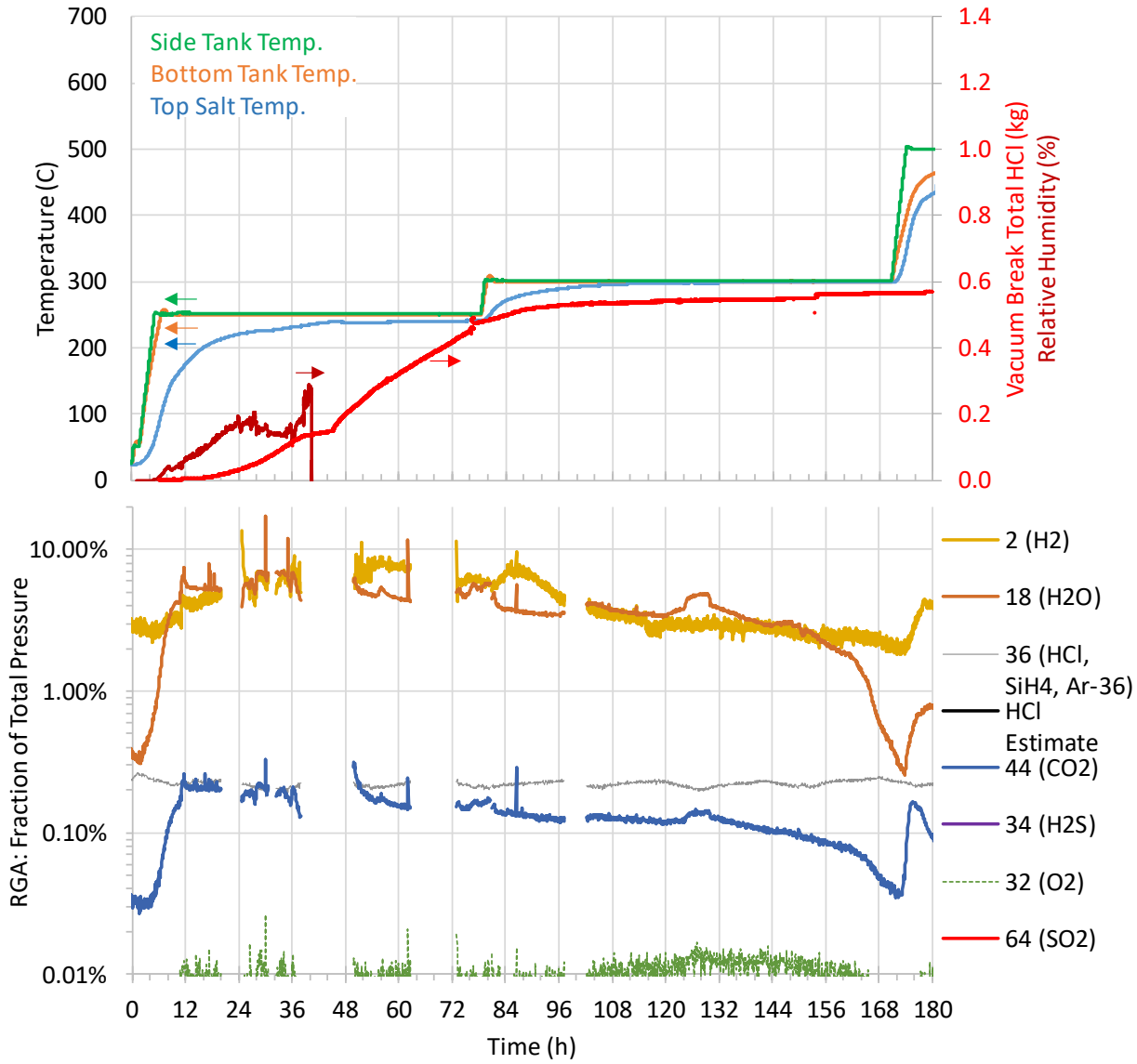

Figure 2. Process data during low-temperature phase.

During the ramp to 250°C, droplet entrainment and carryover between scrubber vessels was observed. To reduce carryover, the total Ar gas flow (i.e., sweep and sparger) was reduced from 6 to 4 slpm. A total flow of 4 slpm into the processing vessel was generally maintained throughout the remainder of the process.

Early during heating, the relative humidity in the effluent stream increased, peaking at 28% before the sensor failed. Before the peak value, the effluent line experienced several minor plugging events that caused the vessel to pressurize (<5 psig) before self-clearing. The effluent line then experienced a more severe and sustained plugging event from 36.2 to 45.4 h. The plug is suspected to have occurred in the nonheated section of tubing between the heated effluent line and the scrubbers. Among the condensed humidity, white crystals were observed to form in this section of line. During the sustained plugging event, the processing vessel pressure increased, and it is suspected that HCl condensed and corroded the humidity sensor to the point of failure. Interestingly, after the line self-cleared, the effluent line did not experience any more issues throughout the remainder of the process.

The first and second scrubbers were drained and refilled toward the end of the 250 and 300°C holds at 76.5 and 153.7 h, respectively. Not accounting for any evaporation from the scrubbers, 3.73 kg of additional water were recovered from the first two scrubbers after the end of the 250°C hold, whereas only 0.10 kg of additional water was recovered during the 300°C hold. Thus, the bulk of water release from the salt occurred during the 250°C hold.

HCl is the byproduct of hydrolysis reactions forming MgOHCl. The amount of HCl collected in the first scrubber, as plotted in Figure 2, was calculated based on the in situ measurement of HCl concentration and the estimated amount of water in the scrubber. The amount of water in the scrubber was assumed to vary linearly between the initial amounts loaded and the final amounts recovered. Significant HCl was generated during the 250°C hold. In contrast, the 300°C hold yielded only minor additional HCl. Based on the analytical analysis of the scrubber samples, 535 g of HCl were captured in first two scrubbers during the 250°C hold, whereas 121 g were captured during the 300°C hold. For both the online sensor monitoring for the first scrubber tank and the sample analysis, most of the HCl was released during the 250°C hold rather than the 300°C hold.

The output from the RGA is plotted in Figure 2. The quadrupole mass spectrometer (QMS) provides signals of a mass-to-charge ratio (m/Z). Figure 2 includes examples of the species for the measurements; however, there may be alternate species not listed for some ratios. The RGA also occasionally tripped due to internal pressure limits. Later, the RGA ran reliably for extended periods. The SO_2, O_2, H_2S were all detected at concentrations below the range of the plot.

Consistent with the humidity sensor, the RGA detected an increase in the effluent moisture concentration early during heating. The moisture level steadily decreased over the next 144 h before dropping precipitously. The detected H_2 largely followed the trends of the moisture. However, the background of H_2 in the system can stem from the RGA unit itself and be due to the difficulty of compressing H_2 via the turbo pump. The lower levels of CO_2 detected may be attributed to gas trapped in the salt pile during loading. The CO_2 concentration decreased over time.

The 36 m/Z RGA signal can be attributed to HCl, ^{36}Ar, and SiH_4. Argon-36 is present at concentrations of 0.3% of the ^{40}Ar peak [18]. Because Ar was used as the sparging and cover gas, a significant fraction of the RGA's signal for 36 m/Z can be attributed to ^{36}Ar. In an attempt to account for this, the "HCl Estimated" trend is the result of subtracting of 0.3% of the 40 m/Z signal from the 36 m/Z signal, which reduces the 36 m/Z signal by the expected concentration of ^{36}Ar. Despite HCl being captured in the scrubber, the correction for ^{36}Ar is predicted to account for most of the 36 m/Z signal and is below the scale shown in Figure 2.

The humidity detected by the RGA greatly decreased around 162 h, suggesting that the 300°C hold was reaching the limit of its efficacy in driving off chemically bound water. Furthermore, the collection of HCl in the scrubber had plateaued. These two signals motivated proceeding to the high-temperature phase of the process.

3.3 HIGH-TEMPERATURE PROCESS

The high-temperature stage of the purification process involved melting the salt and contacting the salt with Mg metal. Measurements of off-gas and other instrumentation were continued during this stage; but, with the salt in the molten state, monitoring from the electrochemical sensor could also be initiated. Prior to the initiation of the purification procedure, the endpoint for the reactive metal contacting step was set to be when the salt redox potential, as measured by the installed electroanalytical sensor, achieved a value lower than 0.85 V vs Mg^0/Mg^{2+}. A potential this low indicates that the major corrosion products and corrosive impurities are all at very low levels [19].

During the ramp from 300 to 500°C, the CO_2, H_2O and H_2 concentration increased in the process effluent, as shown in Figure 3. In addition to this data, the temperature plateau and fluctuation for the thermocouple near the top of the salt provides evidence of salt melting. Once molten Mg(OH)Cl can contact and consume the Mg initially added to the salt, H_2 is generated, as shown in Eq. (6). The H_2 generation peak is reached at 187 h and then begins to slowly decline. Dehydration of $MgCl_2 \cdot H_2O$, as shown in Eqs. (2) and (4), and low temperature thermal decomposition of MgOHCl, as shown in Eq. (5), results in the release of HCl. As the H_2 generation began decreasing at 187 h, the rate of HCl collection in the first scrubber increased, averaging 0.8 g/h during 171–187 h and 2.7 g/h during 187–204 h. Around 198 h when the top of the salt reached approximately 500°C, the RGA signal for 36 amu m/z increases. Thus, while heating the salt to 500°C, there was an initial period of Mg interaction and consumption, releasing H_2, that gradually transitioned to HCl generation. Even with the initial Mg metal added to the salt, the first measurement of redox potential for the salt was approximately 2.0 V vs Mg^0/Mg^{2+}. Potentials in this range are consistent with the presence of significant quantities of HCl in the salt.

The bubbler line plugged three times at process times of 204.7–216.9 h, 232.6–246.6 h, and 265.8–270.5 h. The line was unplugged each time by inserting a rod through the bubbler. All plugs were found to reside near the exit of the bubbler line. After the line was cleared at 216.9 h, the re-agitation of the salt temporarily increased the HCl and H_2O RGA signal. During the second plugging event, the process temperature was increased from 500 to 550°C, trace heating was added to the preheat the gas in the line, and the bubbler flow rate was increased from 1.5 to 2.0 slpm after the plug was removed. By increasing the temperature and flow rate, the gas velocity increased from approximately 0.76 to 1.1 m/s. Unclogging the line and re-agitation of the salt at 246.6 h caused the fluctuation in the temperature near the top of the salt and the increase in the RGA HCl, CO_2, and H_2O signal, as shown in Figure 3. Despite the process changes, a third plugging event occurred. No additional process parameters were modified in response to the event; however, no further plugging events occurred after this event. A definitive cause for the plugging events was not discerned. However, it is suspected the gas may not have been sufficiently preheated and resulted in salt freezing local to the bubbler tube discharge.

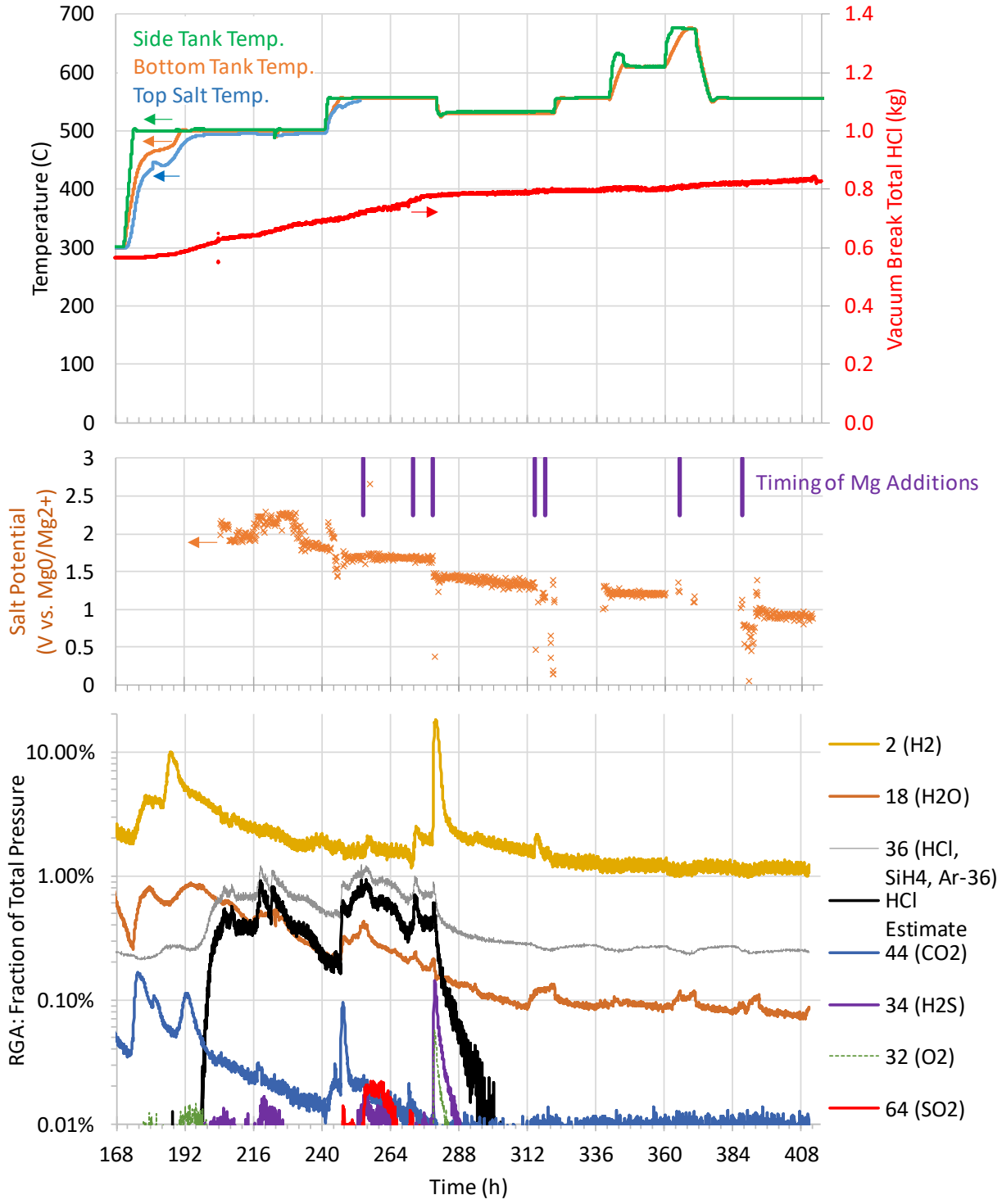

Figure 3. Process data during high-temperature phase.

After the resolution of the second plugging event, the measured salt redox potential was still higher than desired (1.6–1.7 V vs. Mg^0/Mg^{2+}). The steady H_2 RGA signal, the elevated HCl RGA signal, and the steady climb in the scrubber HCl concentration suggested that the MgOHCl was no longer interacting with Mg and that the process was instead progressing with the undesirable thermal decomposition of MgOHCl. In response, more Mg was added to the salt. The additions were made at six times at approximately three different vessel temperatures. In addition to the 241 g of Mg initially loaded with the salt, 243 g of Mg were added to the salt during the process. The Mg additions and a summary of the observed system response are summarized in Table 2.

Table 2. Magnesium addition schedule and response summary.

Process time (h)	Vessel temp. (C)	Mg added (g)	Observed RGA and scrubber response	Observed electrochemical sensor response
254.6	558	69.2	Increase in H_2, HCl, and H_2O. SO_2 appears.	Minor change
271.8	558	37	Increase in H_2 and HCl.	Minor change
278.6	557	69	Significant increase in H_2 generation. Decrease in HCl RGA signal. Small spike in H_2S and O_2. Decrease rate of HCl capture in scrubber throughout remainder of process.	Step change down
314.3	533	16	Increase in H_2 and H_2O.	Minor change down
318.1	533	18	Increase in H_2 and H_2O.	
365.0	676	12.3	Increase in H_2O.	Larger change down
386.8	556	21.9	Increase in H_2O.	

The first addition resulted in minor increases in H_2 and HCl. Interestingly, the signal for SO_2 also appeared. The H_2, H_2O, HCl, CO_2, and SO_2 signals decreased over time; however, the salt redox potential remained consistent. The second addition caused a response similar to the first but without the presence of SO_2. The third addition resulted in a significant increase in H_2. In response, the process temperature was decreased to 530°C, and the sweep gas flow rate increased. In addition to H_2, spikes in the signal for H_2S and O_2 occurred. Conversely, the HCl RGA signal and the rate of HCl capture in the scrubber dropped precipitously. Although the first and third additions were similar in mass, they resulted in substantially different process responses. After the third addition, there was a step change in the salt redox potential down to approximately 1.4 V vs. Mg^0/Mg^{2+}. Raw electroanalytical signals from the electrochemical sensor during this period of time are shown in Figure 4. The Mg additions resulted in quantifiable changes to hydroxide and metal ion concentrations. Less Mg was added during the fourth and fifth additions. These additions caused a minor increases in H_2 and H_2O (Figure 3) and further decreases in MgOH+ and anion content (Figure 4). At this point, the system was brought to 675°C, which is above the melting point of Mg (650°C). During heating, the RGA and electrochemical probe readings remained steady, and no unique signature was identified, bringing the system above 650°C. One Mg addition was made while the system was at high temperatures before returning the system to 550°C.

The time evolution of the salt redox potential during the Mg additions is shown in Figure 5. The final Mg addition decreased the redox potential to 0.89 V vs. Mg^0/Mg^{2+}. With the low salt redox potential, the low and steady HCl capture rate in the scrubber, and only minor changes to the RGA signals due to further Mg addition, the purification process was deemed complete, and preparations for salt transfer were initiated.

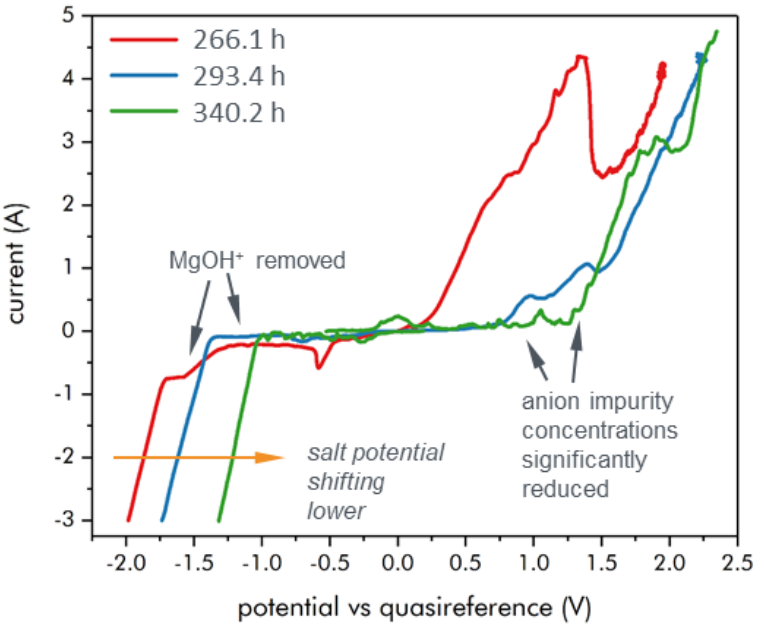

Figure 4. Linear sweep voltammograms during the purification process. Voltammograms were taken in positive and negative directions starting from 0 V vs. OCV.

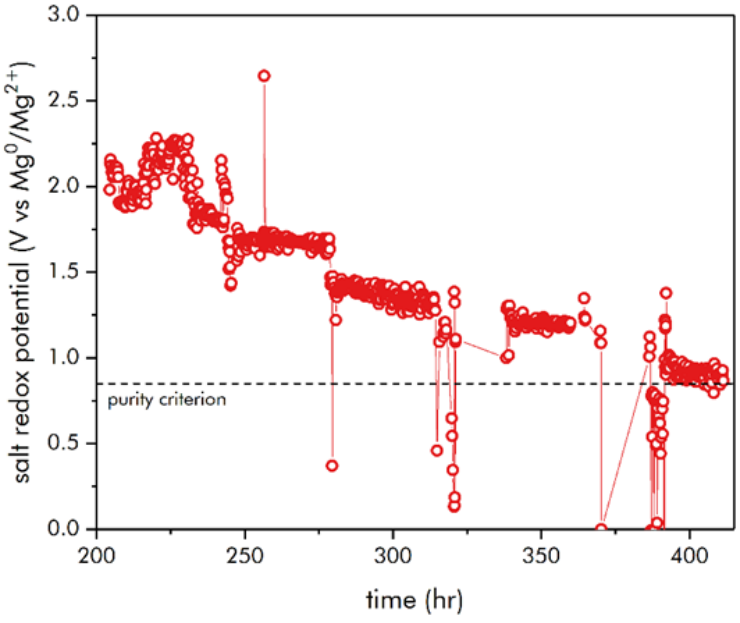

Figure 5. Salt redox potential versus time during reactive metal contacting process.

3.4 SALT TRANSFER

Upon completion of the chemical purification stage, the gas flow rate through the sparging tube was reduced to 0.25 slpm at 392 h. This lower flow rate permitted MgO and other particulates to settle for 23 h before initiating salt transfer.

A transfer tube was inserted to approximately 5 cm (2 in.) above the bottom of the processing vessel liner. Using a nearly constant pressure differential between the tanks, the salt was transferred through the heated line and through the three filters. The mass transferred was measured by the scale located under the storage tank. Transferring 194.1 kg of salt at 555–565°C took approximately 10.3 h. During the first half hour, the transfer rate was approximately 2.25 kg/min. The transfer rate then decreased over time from approximately 0.38 kg/min to 0.16 kg/min, suggesting that the filters collected debris during transfer. However, the filters appeared clean during post-use inspection, and particulates could not be identified using a microscope. At the end of the transfer, gas from the processing vessel flowed through the line into the storage tank. During this transient, salt could have drained back into the processing vessel and carried filter debris with it. Although debris was not found within the filters after the transfer, the change in transfer rate suggests that debris was being captured in the filters.

Using the geometry of the processing vessel liner, the submerged height of the transfer tube, and an assumed salt density of 1,648 kg/m^3, 14.1 kg of salt are estimated to remain in the bottom of the crucible. By comparing the amount of salt initially loaded (212.2 kg) and the Mg added (0.485 kg) with the amount transferred (194.1 kg) and the estimated amount remaining in the liner after transfer (14.1 kg), approximately 4.5 kg were lost from the salt during the process. This equates to 2.12 wt % of the initial loaded salt.

4. POST-PROCESS ANALYSIS

4.1 SALT SAMPLE COMPOSITION

The compositions of six salt samples were analyzed to assess the success of the purification process. The three major salt constituents (i.e., Na, K, and Mg) were analyzed using inductively coupled plasma (ICP) mass spectrometry (MS), and 52 other elements were detected using ICP optical emission spectrometry. The composition results for four of the samples are provided in Table 3. Table 3 excludes elements that were detected at levels below 1 ppm (i.e., Be, Sc, V, Cu, Zn, As, Y, Zr, Nb, Rh, Pd, Ag, Cd, Sn, Sb, Cs, La, Ce, Pr, Nd, Sm, Eu, Dy, Ho, Yb, Lu, Hf, Ta, Pt, Hg, Tl, Pb, Th, U). Two samples—one each from the AC and halite salts prior to purification—were taken and analyzed. Based on the mass of each salt loaded into the purification vessel, the weighted composition of the starting salt blend is also provided in Table 3. Two samples were taken during the transfer of the salt from the processing vessel to the storage vessel. The sample location was situated before the salt passed through the filters. Transfer sample 1 was captured in a tee section in-line with the transfer tube, whereas transfer sample 2 was taken from residual salt remaining inside the line after transfer. The average of the two transfer line samples is also shown in Table 3. The measurement uncertainty ranges for the four samples are summarized in the final column. The measurements indicate a decrease in all minor impurities, except Se, Ni, Cr, and W.

Table 3. Salt sample composition.

Element	Halite (ppm)	AC (ppm)	Weighted start (ppm)	Transfer sample 1 (ppm)	Transfer sample 2 (ppm)	Transfer average (ppm)	Percent change start-end (%)	Measurement uncertainty (±%)
K	47,369	189,987	**180,914**	202,676	195,061	**198,869**	10	2.0–2.2
Mg	483	109,952	**102,988**	110,508	107,684	**109,096**	6	1.6–1.9
Na	338,526	50,534	**68,856**	74,423	71,163	**72,793**	6	1.9–2.5
Ca	6,377	1,516	**1,825**	1,295	1,333	**1,314**	–28	1.0–2.6
S	11,496	148	**870**	283	371	**327**	–62	0.6–1.8
Fe	316	359	**356**	1.2	2.8	**2.0**	–99	1.5–3.8
Rb	85	310	**296**	227	234	**231**	–22	1.3–3.4
Sr	108.3	25.6	**30.9**	21.8	22.5	**22.2**	–28	1.4–2.1
Al	428.3	1.5	**28.6**	1.6	1.8	**1.7**	–94	1.3–2.8
B	362.4	1.7	**24.7**	1.2	0.8	**1.0**	–96	0.9–6.4
Se	0.5	24.6	**23.1**	41.3	33.3	**37.3**	61	2.4–9.4
Mn	8.3	7.1	**7.2**	3.1	0.4	**1.8**	–75	0.8–2.2
Li	34.9	3.3	**5.3**	3.5	3.9	**3.7**	–30	1.9–2.6
P	15.3	1.3	**2.2**	0.4	0.3	**0.3**	–84	1.7–13.3
Ti	17.4	0.2	**1.3**	0.1	0.1	**0.1**	–92	2.0–29.1
Ba	5.1	1.0	**1.3**	1.1	1.2	**1.1**	–13	0.9–4.1
Ni	0.2	0.5	**0.5**	1.3	14.8	**8.0**	1,452	1.0–5.6
Cr	0.3	0.5	**0.5**	5.8	3.7	**4.7**	845	7.0–24.0
W	0.05	0.01	**0.01**	0.81	2.47	**1.64**	11,770	0.9–3.0

The salt compositions for the samples are summarized in Table 4 and assume that the major salt constituents are in the form of chloride salts. The "Other Measured" category is the summation of the other 51 elements measured and does not try to account for their molecular form (e.g., oxide, hydroxide, chloride). The "Balance" category includes species not measured (e.g., moisture). The fraction of major salt constituents increased during the process, which was expected because moisture, hydroxides, and minor species (Table 3) were removed from the salt. Considering only the major salt constituents, the variation in the initial salt blend (18.9NaCl-37.2KCl-43.4$MgCl_2$-0.5$CaCl_2$, wt %) was within the uncertainty of the measurements of the composition transferred to the storage tank (18.6NaCl-38.1KCl-42.9$MgCl_2$-0.4$CaCl_2$, wt %). This discussion assumed that the Mg detected is in the form of $MgCl_2$. Some of the Mg is likely in the form of MgO and not $MgCl_2$, both in the pre- and post-process salts. An initial concern for the process was the potential for volatilization and loss of a salt species sufficient enough to shift the composition. However, the results suggest that a disproportionate amount of one salt species was not volatilized from the process.

Table 4. Salt sample composition assuming major components are in the form of chloride salt.

Constituent	Halite (wt %)	AC (wt %)	Weighted start (wt %)	Transfer sample 1 (wt %)	Transfer sample 2 (wt %)	Transfer average (wt %)
NaCl	86.1	12.8	**17.5**	18.9	18.1	**18.5**
$MgCl_2$	0.2	43.1	**40.3**	43.3	42.2	**42.7**
KCl	9.0	36.2	**34.5**	38.6	37.2	**37.9**
$CaCl_2$	1.77	0.42	**0.51**	0.36	0.37	**0.36**
Other measured	1.29	0.09	**0.17**	0.06	0.07	**0.06**
Balance	1.67	7.35	**6.99**	–1.27	2.09	**0.41**

The evolution of metal content in the salt provides some insight into the process. The crucible and sparger tube were made of alloy C-276, the nominal composition of which is provided in Table 5. Excluded from the table are the minor alloying elements present at concentrations below 0.35 wt % (i.e., V, Si, P, S, C). Included in Table 5 are the estimated compositions from Table 4 of the initial salt, before purification, and the transferred salt. The fifth column is the measured composition of a sample taken from the salt remaining in the purification vessel after salt transfer, termed *Sludge*. The final column is an estimate of the salt composition before salt transfer (i.e., a weighted average of the transferred salt samples and sludge sample compositions).

Table 5. Metal species measured in the salt.

Element	Alloy C-276 (wt %)	Initial salt (ppm)	Transferred salt (ppm)	Sludge (ppm)	Estimated end salt (ppm)
Ni	Balance	0.52	8.01	11.40	8.24
Mo	15.0–17.0	0.23	0.43	3.03	0.61
Cr	14.5–16.5	0.50	4.75	13.23	5.32
Co	2.5 max	0.06	0.01	0.06	0.01
W	3.0–4.5	0.01	1.64	2.15	1.67
Fe	4.0–7.0	356.24	1.98	36.69	4.34
Mn	1.0 max	7.22	1.78	2.42	1.82

Molten halide salts preferentially attack the Cr within metal alloys [6, 13, 14]. An increase of Cr in the salt would be expected during the purification process. The combined AC and halite salt initially loaded contained approximately 0.1 g of Cr based on the sample analysis. After the process, the salt is estimated to have contained 1.1 g of Cr. The increase of 1.0 g of Cr in the salt equates to approximately 0.94 μm of

Cr depletion in the C-276 alloy. This assumes that the C-276 alloy contains 15.5 wt % Cr and a salt wetted contact area of 1.29 m^2. Although this suggests that the crucible experienced little corrosion during the process, there are several complicating factors. First, it does not account for the redeposition of corrosion products. Second, it does not reflect corrosion that may have occurred in the gas space of the vessel. Conversely, corrosion products from the upper portions of the vessel (i.e., not salt contacted) could have relocated into the salt during the process. Noting its limitations, the salt Cr composition does not suggest extensive corrosion of the crucible during the process.

In contrast to Cr, the elements Ni, Mo, Co, and W are less susceptible to corrosion. The source salt and the post-process salt contained little Mo, Co, and W. The concentration of Ni increased; however, the crucible is approximately 57% Ni, and such an increase (i.e., approximately 1.7 g) is not unexpected.

Iron is in between Cr and the other more corrosion resistant metals. Both the Halide and AC salts initially contained Fe, averaging 356 ppm for the loaded blend (i.e., 75.6 g). Based on the two samples of the transferred salt, the concentration was only 2 ppm of Fe (i.e., 0.4 g). The sludge sample contained 37 ppm of Fe (i.e., approximately 0.5 g). However, the measurements cannot account for the location of 74.7 g of Fe. Suspected locations include settling the Fe within the sludge so that the sample was not representative of the total Fe present or deposition of Fe onto the vessel. A reduction in Fe content in the purified salt was also observed in Zhao [15], which used quartz crucibles.

4.2 SCRUBBER CONTENTS COMPOSITION

The concentrations of impurities in samples from the scrubbers were analyzed using ICP-MS (K, Mg, Na, Ni, Cr, Fe, Ca, S, Si) and ion chromatography (Cl-, Br-). Figure 6 illustrates the capture of salt species in each of the four scrubbers and the time evolution of capture in the first two scrubbers. Similarly, Figure 7, presents the data for the metallic species, and Figure 8 provides the data for Cl.

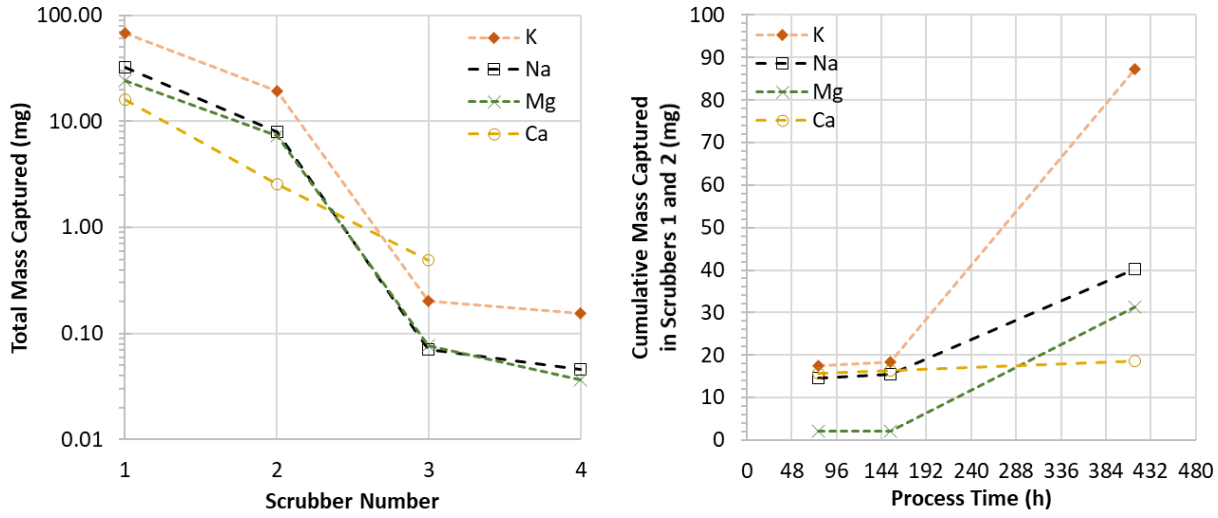

Figure 6. Salt species captured in the scrubbers.

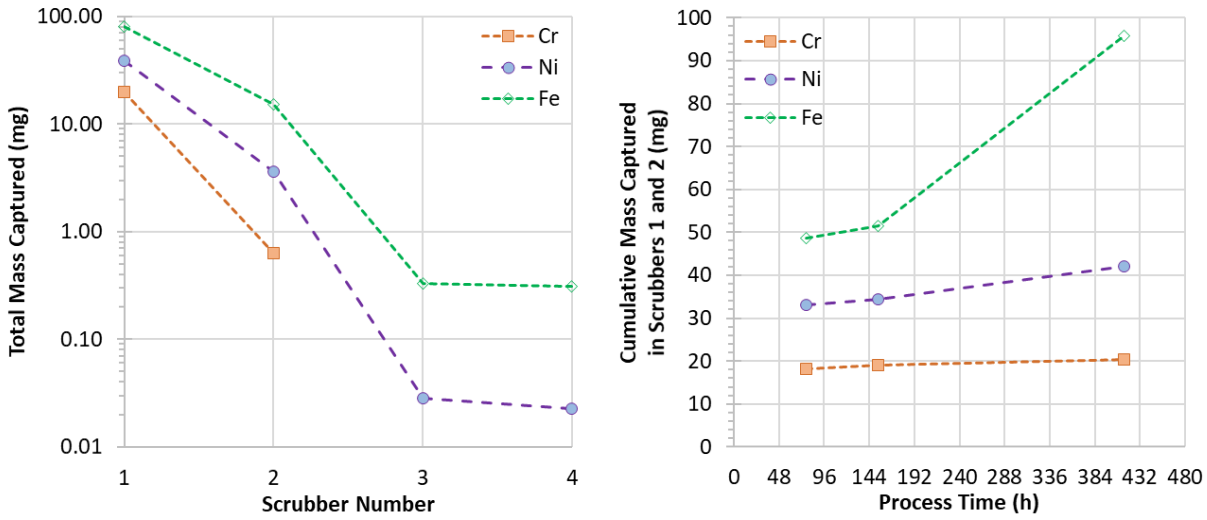

Figure 7. Metal species captured in the scrubbers.

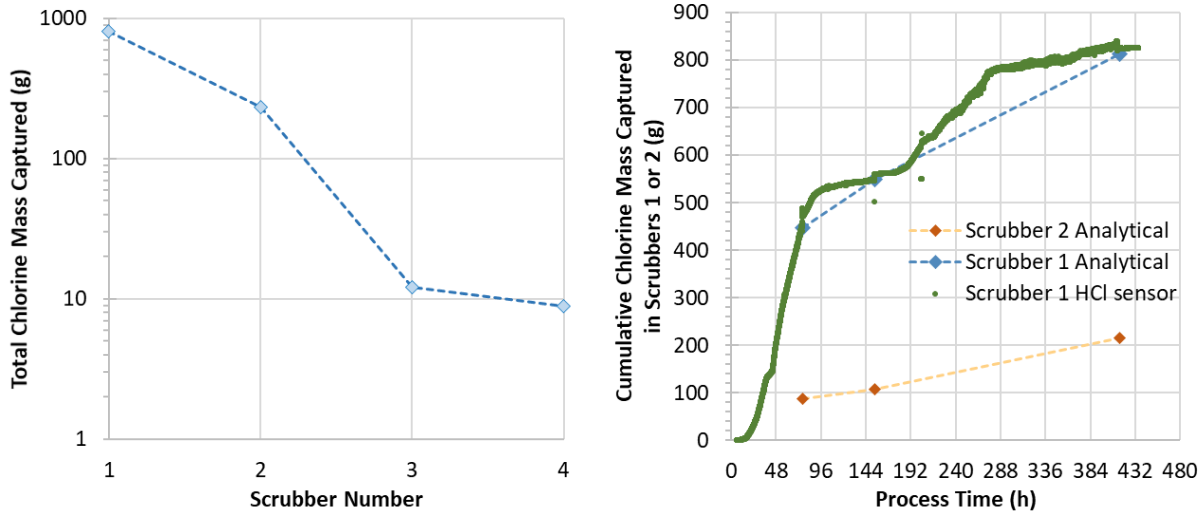

Figure 8. Chlorine captured in the scrubbers.

One concern for the process was the vapor pressure and potential volatilization of the salt species. If excessive, then the salt may deposit and plug the effluent lines and/or cause a shift in the salt composition. As indicated in Figure 6, a small amount of salt species was transported to and captured by the scrubbers. Assuming that the species were in the form of chloride salts, 0.45 g (0.0002 wt % of the initial salt) was captured in the scrubbers. Following expectations, more K, Mg, and Na relocated to the scrubber during the high-temperature phase of the process rather than the low-temperature phase; however, the amount was still low.

The effluent line plugged several times early in the process before the salt was molten. As noted, crystals appeared in the line. However, only 0.12 g of salt species is estimated to have been captured in the first two scrubbers when they were drained and refilled at 76.5 h. This small amount of salt is insufficient to plug the line sizes used. The species responsible for plugging the effluent line remains unclear.

The Fe, Cr, and Ni captured in the scrubbers (Figure 7) are attributed to corrosion. The Cr concentration in the third and fourth scrubbers were less than the 0.003 ppm detection limit. Most of the metal species appeared early in the process during which there were elevated releases of HCl in the presence of moisture. Products from corrosion in the effluent line would drain downward into the scrubbers. The higher Fe content may be attributed to the stainless-steel fittings used to connect the humidity sensor and RGA to the C-276 effluent line. Like the salt species, minor metallic species were found in the scrubber (i.e., 0.16 g total).

For the first two scrubbers, the concentrations of Si and S were below the detection limit of 0.1 ppm. Although Si was below the detection limit of 0.22 ppm in the third and fourth scrubber, S was detected at concentrations of less than 1 ppm.

Only the last samples from the four scrubbers were analyzed for Br. The first scrubber contained 371 ppm, and scrubbers 2, 4, and 4 contained 138, 9, and 3 ppm, respectively. Of the species investigated, and excluding Cl, Br was the most prevalent impurity detected in the scrubber with at least 1.45 g captured. Because the first two drain/refills of the first and second scrubbers were not analyzed, an overall mass balance could not be performed. Although the Br concentration of the starting salt was not analyzed, a concentration of 3,900 ppm was reported in Zhao and Vidal [3] for a similar batch of the ICL AC.

The total Cl captured in each scrubber is shown in Figure 8. Consistent with the results for the salt and metallic species, the scrubber effectively captured Cl. The ion chromatography analytical measurement of Cl concentration in the scrubber samples were compared against the HCl sensor measurements. For the six samples compared, the variations in concentration were within the uncertainty of the measurements. This provides confidence the HCl sensor, and data remained accurate throughout the process; thus, the HCl trends shown in Figure 2 and Figure 3 are accurate.

The scrubbers do not capture the O_2, H_2, and CO_2 detected by the RGA in the effluent. If all 485 g of Mg reacted with MgOHCl, then the resulting H_2 released would be 40 g.

An 3.25 kg increase of liquid was recovered from the scrubbers compared with the amount added. Based on the analytical results for Cl concentration, the scrubbers captured an estimated 1.05 kg of HCl (0.50 wt % of the salt). Subtracting this amount from the liquid collected indicates that 2.2 kg of water were condensed and collected in the scrubbers. However, given the long process, water would have evaporated from the scrubbers. Using the Ar flow rates and measured scrubber temperature, and assuming the Ar was fully saturated before venting, approximately 1.93 kg of water may have evaporated and been removed from the scrubber by the Ar flow. With the capture and evaporation estimates, approximately 4.13 kg of water were released by the salt (i.e., 1.94 wt % of the salt).

The estimated water and HCl driven off the salt from the process represent 2.44 wt % of the initial salt mass. This is corroborated by the estimate of 2.12 wt % lost based on a mass balance. Given the uncertainty and limitations in the measurements, particularly the amount of material remaining in the crucible and the amount of water evaporated from the scrubber, these mass loss estimates are deemed close.

5. SUMMARY OF FINDINGS

Experience and insight from the process includes the following.

- The process successfully purified approximately 200 kg of salt, as confirmed by ICP-MS compositional analysis of the salt, measurement of the salt redox potential, and the stability of effluent composition as measured by the RGA.
- The salt required a 0.23 wt % addition of Mg to lower the salt redox potential to the purity criterion of 0.89 V vs. Mg^0/Mg^{2+}.
- A majority of the HCl (51%) and moisture (75%) were driven off the salt during the 250°C hold. In contrast, the subsequent 300°C hold only contributed minor additions to the total HCl (11%) and moisture (5%) released. The high-temperature portion of the process released the remainder of the HCl (38%) and moisture (20%).
- The in situ measurement of HCl concentration in the scrubber, the RGA species data, and the salt redox potential measurements provided unique insight into the process. During melting, H_2O, CO_2, and H_2 were released, likely due to the reaction with the Mg initially loaded with the salt. After melting, initial in situ Mg additions resulted in differing presence and magnitude of species released. Early additions resulted in H_2, H_2O, HCl, SO_2, H_2S, and O_2 being released. Later additions resulted in lowering the redox potential but only resulted in minor changes to the RGA species detected.
- Based on ICP-MS measurements, the concentration of 12 species (i.e., Ca, S, Fe, Rb, Sr, Al, B, Mn, Li, P, Ti, Ba, Co) decreased because of the process. The concentration of four minor impurity species (i.e., Se, Cr, Ni, W) increased because of the process. The increases of Cr and Ni are attributed to minor corrosion in the processing vessel. Of the Fe initially present in the salt blend, 74.7 g were unaccounted for in the salt measurements after the process. The Fe is suspected to have deposited onto the process crucible.
- An estimated 1.94 wt % water and 0.50 wt % HCl were released from the salt.
- A disproportionate amount of a single salt species was not volatilized from the process.

Recommendations for future processing are as follows.

- Oxidation and consumption of pre-loaded Mg may occur during the early thermal dehydration of the salt. Nonreacted Mg will interact and lead to the release of H_2 upon salt melting. Pre-loading Mg into the salt requires careful thought when scaling the process.
- Bromine should be included as an impurity to measure in the pre- and post-process salt. It is also an impurity present in the process effluent.
- The gas entering the bubbler line should be preheated above the salt freezing temperature. Direct monitoring of the gas temperature is recommended.
- The relative humidity sensor reliability may be extended by intermittently sampling the acidic effluent instead of continuous exposure.
- The high-temperature phase of the process may be accelerated with more frequent Mg additions.
- It is recommended that the purification process be conducted at 550°C in contrast to a higher-temperature process above the melting point of Mg (650°C).

6. ACKNOWLEDGMENTS

The development of the purification facility and process benefitted from the efforts of many individuals, including Ricardo Muse, Kurt Smith, Joanna McFarlane, and David Felde at ORNL. Insight from previous smaller-scale purification efforts were provided by Youyang Zhao and Judith Vidal at National Renewable Energy Laboratory, as well as Mark Anderson at the University of Wisconsin. The salt reagents were donated by Albemarle Inc. and ICL.

This material is based upon work supported by the US Department of Energy's Office of Energy Efficiency and Renewable Energy under Solar Energy Technologies Office agreement number 33875.

7. REFERENCES

1. K. R. Robb, P. L. Mulligan, G. L. Yoder Jr., K. Smith, and J. Massengale. 2019. *Facility to Alleviate Salt Technology Risks (FASTR): Preliminary Design Report with Failure Modes and Effects Analysis*. ORNL/TM-2019/1370. Oak Ridge National Laboratory, Oak Ridge, Tennessee.
2. G. J. Kipouros and D. R. Sadoway. 1987. "The Chemistry and Electrochemistry of Magnesium Production." *Advances in Molten Salt Chemistry* 6: 127–209.
3. Y. Zhao and J. Vidal. 2020. "Potential Scalability of a Cost-Effective Purification Method for $MgCl_2$-Containing Salts for Next-Generation Concentrating Solar Power Technologies." *Solar Energy Materials and Solar Cells* 215: 110663.
4. R. T. Mayes, J. M. Kurley III, P. W. Halstenberg, A. McAlister, D. Sulejmanovic, S. Raiman, S. Dai, and B. A. Pint. 2018. *Purification of Chloride Salts for Concentrated Solar Applications*. ORNL/LTR-2018/1052. Oak Ridge National Laboratory, Oak Ridge, Tennessee.
5. J. M. Kurley, P. W. Halstenberg, A. McAlister, S. Raiman, S. Dai, and R. T. Mayes. 2019. "Enabling Chloride Salts for Thermal Energy Storage: Implications of Salt Purity." *RSC Advances* 9(44): 25602–25608.
6. J. W. Ambrosek. 2011. *Molten Chloride Salts for Heat Transfer in Nuclear Systems*, PhD dissertation, University of Wisconsin—Madison.
7. J. McFarlane, G. D. Del Cul, J. R. Massengale, R. T. Mayes, K. R. Robb, and D. Sulejmanovic. 2022. "Chloride Salt Purification by Reaction with Thionyl Chloride Vapors to Remove Oxygen, Oxygenated Compounds, and Hydroxides." *Front. Chem. Eng*. 4: 811513. doi: 10.3389/fceng.2022.811513.
8. C. J. Raseman, H. Susskind, G. Farber, W. E. McNulty, and F. J. Salzano. 1960. *Engineering Experience at Brookhaven National Laboratory in Handling Fused Chloride Salts*. BNL-627. Brookhaven National Laboratory, Upton, New York.
9. T. R. Johnson, F. G. Teats, and R. D. Pierce. 1969. *A Method for the Purification of Molten Chloride Salts*. ANL-7603. Argonne National Laboratory, Lemont, Illinois.
10. D. L. Hill, J. Perano, and R. A. Osteryoung. 1960. "An Electrochemical Study of Uranium in Fused Chlorides." *Journal of the Electrochemical Society* 107.8: 698.
11. B. L. Garcia-Diaz et al. 2016. "High Temperature Electrochemical Engineering and Clean Energy Systems." *Journal of the South Carolina Academy of Science* 14.1: 4.
12. S. Choi, N. E. Orabona, O. R. Dale, P. Okabe, C. Inman, and M. F. Simpson. 2019. "Effect of Mg Dissolution on Cyclic Voltammetry and Open Circuit Potentiometry of Molten $MgCl_2$–KCl–NaCl Candidate Heat Transfer Fluid for Concentrating Solar Power." *Solar Energy Materials and Solar Cells* 202: 110087.
13. B. A. Pint. 2020. *Progression to Compatibility Evaluations in Flowing Molten Salts*. ORNL/SPR-2020/1490. Oak Ridge National Laboratory, Oak Ridge, Tennessee.
14. W. Ding et al. 2019. "Molten Chloride Salts for Next Generation Concentrated Solar Power Plants: Mitigation Strategies against Corrosion of Structural Materials." *Solar Energy Materials and Solar Cells* 193: 298–313.
15. Y. Zhao. 2020. *Molten Chloride Thermophysical Properties, Chemical Optimization, and Purification*. NREL/TP-5500-78047. National Renewable Energy Laboratory, Golden, Colorado.
16. B. A. T. Mehrabadi et al. 2017. "Modeling the Effect of Cathodic Protection on Superalloys inside High Temperature Molten Salt Systems." *Journal of the Electrochemical Society* 164.4: C171.
17. G. Mohan, M. Venkataraman, J. Gomez-Vidal, and J. Coventry. 2018. "Assessment of a Novel Ternary Eutectic Chloride Salt for Next Generation High-Temperature Sensible Heat Storage." *Energy Conversion and Management* 167: 156–164.

18. W. E. Wallace. “Mass Spectra” from *NIST Chemistry WebBook*. NIST Standard Reference Database Number 69, eds. P. J. Linstrom and W.G. Mallard. National Institute of Standards and Technology, Gaithersburg, Maryland, 20899. Accessed April 14, 2022. doi: 10.18434/T4D303.
19. J. Guo, N. Hoyt, M. Williamson. “Multielectrode Array Sensors to Enable Long-Duration Corrosion Monitoring and Control of Concentrating Solar Power Systems.” *Journal of Electroanalytical Chemistry* 884 (2021).